HHS Public Access

Author manuscript

Brain Stimul. Author manuscript; available in PMC 2022 June 06.

Published in final edited form as:

Brain Stimul. 2022 ; 15(1): 190–196. doi:10.1016/j.brs.2021.12.005.

High resolution ultrasonic neural modulation observed via *in vivo* two-photon calcium imaging

Zongyue Cheng[a,b], **Chenmao Wang**[a,b], **Bowen Wei**[a,b], **Wenbiao Gan**[c], **Qifa Zhou**[d], **Meng Cui**[a,b,e,*]

[a]School of Electrical and Computer Engineering, Purdue University, West Lafayette, IN, 47907, USA

[b]Bindley Bioscience Center, Purdue University, West Lafayette, IN, 47907, USA

[c]Skirball Institute, Department of Neuroscience and Physiology, Department of Anesthesiology, New York University School of Medicine, New York, NY, 10016, USA

[d]Department of Biomedical Engineering and Department of Ophthalmology, University of Southern California, Los Angeles, CA, 90089, USA

[e]Department of Biology, Purdue University, West Lafayette, IN, 47907, USA

Abstract

Neural modulation plays a major role in delineating the circuit mechanisms and serves as the cornerstone of neural interface technologies. Among the various modulation mechanisms, ultrasound enables noninvasive label-free deep access to mammalian brain tissue. To date, most if not all ultrasonic neural modulation implementations are based on ~1 MHz carrier frequency. The long acoustic wavelength results in a spatially coarse modulation zone, often spanning over multiple function regions. The modulation of one function region is inevitably linked with the modulation of its neighboring regions. Moreover, the lack of *in vivo* cellular resolution cell-type-specific recording capabilities in most studies prevents the revealing of the genuine cellular response to ultrasound. To significantly increase the spatial resolution, we explored the application of high-frequency ultrasound. To investigate the neuronal response at cellular resolutions, we developed a dual-modality system combining *in vivo* two-photon calcium imaging and focused ultrasound modulation. The studies show that the ~30 MHz ultrasound can suppress the neuronal activity in awake mice at 100-mm scale spatial resolutions, paving the way for high-resolution ultrasonic neural modulation. The dual-modality *in vivo* system validated through this study

*Corresponding author. School of Electrical and Computer Engineering, Purdue University, West Lafayette, IN, 47907, USA. mengcui@purdue.edu (M. Cui). Correspondence and requests for materials should be addressed to M.C.

CRediT authorship contribution statement

Zongyue Cheng: Investigation, Data curation, Formal analysis, Writing – original draft, Writing – review & editing. **Chenmao Wang:** Investigation, Data curation, Writing – original draft. **Bowen Wei:** Data curation, Writing – original draft. **Wenbiao Gan:** Supervision, Writing – original draft. **Qifa Zhou:** Supervision, Writing – original draft. **Meng Cui:** Conceptualization, Methodology, Investigation, Supervision, Writing – original draft, Writing – review & editing, Funding acquisition.

Declaration of competing interest

The authors declare no competing financial interests.

Appendix A. Supplementary data

Supplementary data to this article can be found online at https://doi.org/10.1016/j.brs.2021.12.005.

will serve as a general platform for studying the dynamics of various cell types in response to ultrasound.

1. Introduction

Neural modulation technologies hold great significance in neuroscience research and medical applications [1–6]. The capability of exciting or suppressing neuronal activity during behavior can reveal the functions of neural systems and enable brain-machine interfaces [7,8]. Among the various modulation mechanisms, ultrasound-based technologies allow a noninvasive label-free deep penetration in the mammalian brains [9–12], thanks to the weak attenuation of acoustic waves in brain tissue [13–17]. In the majority of applications, low frequency (~1 MHz) ultrasound was employed [18–21]. Despite its wide adoption in neuroscience applications, a limitation of the low-frequency ultrasound is its moderate spatial resolution and confinement [22,23]. The near centimeter-scale modulation zone often covers multiple brain regions, quite coarse for neuroscience research [24]. For neural interface technologies, the large modulation zone also significantly limits the achievable degrees of control. Moreover, the lack of cell-type-specific cellular resolution recording capabilities in most studies poses a significant challenge to uncover the true cellular response to ultrasound.

To drastically improve the spatial resolution and confinement, a straightforward solution would be to reduce the acoustic wavelength [25–33]. Thus, it would be of great significance to access the effect of high-frequency ultrasound on neurons and to investigate the frequency, magnitude, waveform required to achieve reliable neural excitation or suppression [34–43]. In this work, we explored the application of focused ultrasound with near 30 MHz carrier frequency. To evaluate the neuronal activity within the greatly reduced modulation zone at high spatial resolutions, we developed a dual-modality system combining a polymer focused sound transducer and an *in vivo* two-photon fluorescence calcium imaging system, which allowed us to record the activity of neurons at cellular resolutions. Moreover, we employed EEG to monitor the response from neuronal populations.

2. Results

The dual-modality system involves the combination of a two-photon laser scanning fluorescence microscope and a high-frequency focused ultrasound transducer (Fig. 1a). To accommodate the ultrasound transducer (PI35–2-R0.50, Olympus NDT), we employed a water-dipping objective lens (Nikon 16x NA 0.8) with a large access angle. We designed a water container that was attached to a large surface mouse head bar with an O-ring in between (Fig. 1b). The water immersion ensured a proper coupling to the brain tissue for both the light and the sound waves. To minimize the sound reflection, we utilized plastic coverslips as the optical cranial windows, which enabled ~90% acoustic power transmission (Supplementary Table 1). Before *in vivo* imaging, we aligned the ultrasound transducer location such that the ultrasound focus was overlapped with the two-photon imaging focal plane. Experimentally, we mounted fluorescence beads in 2% agar as the calibration sample.

The propagation of the ultrasound wave in agar led to a low-pressure zone which pulled the surrounding beads towards the ultrasound focus by hundreds of nanometers, allowing us to precisely visualize and align the ultrasound focus under the two-photon microscope (Supplementary Fig. 1).

First, we employed the dual-modality system to observe the neuronal response to the 30 MHz continuous wave (CW) ultrasound in the visual cortex of awake mice expressing GCaMP6s. With the ultrasound applied, the calcium transient was significantly reduced (Fig. 1c–e, Supplementary Figs. 1e–g). After the ultrasound was turned off, the calcium transient gradually recovered. To quantify this phenomenon, we performed statistical analysis on the $\Delta F/F_0$. The statistics of 4 mice and 180 neurons show that the presence of the 30 MHz ultrasound can reliably suppress the neuronal calcium activity (Fig. 1f). However, if the mice were under anesthesia with isoflurane (inherently suppressed neuronal activity and calcium transient [44–46]), the effect of ultrasound became insignificant (Fig. 1g). Although the onset of the ultrasound-induced neural suppression was almost instantaneous, the full recovery of the neuronal activity may take over 100 s (Fig. 1h and i).

Next, we investigated using different ultrasound pressure for calcium transient's suppression. Experimentally, we repeated the measurements using different signal amplitude to drive the ultrasound transducer and quantified the ultrasound pressure at the sound focus using a calibrated hydrophone (NH0200, Precision Acoustics). For the recorded calcium signals (Fig. 2a), we statistically quantified the calcium transients' frequency, peak $\Delta F/F_0$, duration, and integrated transient activity for different sound intensities (Fig. 2b–e). The data show that the calcium transient suppression became visible with 20 V CW driving signal (spatial peak temporal average intensity I_{spta}: 2.17 W/cm^2 at sound focus). With the ultrasound turned off, the calcium activities recovered.

The key advantage of the high-frequency ultrasound is the greatly improved spatial resolution and confinement. The employed polymer transducer featured an element size of 6.35 mm in diameter and a focal length of 12.7 mm, resulting in a focal spot of ~170 mm in diameter (Supplementary Fig. 1). By spatially translating the brain, we could study the effect of ultrasound on the same neurons and map the ultrasound neural modulation zone (Fig. 3a and b). Experimentally, a 150 mm horizontal shift could result in an apparent reduction of neuronal modulation effect (Fig. 3c and d), which was comparable to the ultrasound focus spot size.

Next, we explored the implementation of different carrier frequencies and waveforms. Within the ~20 MHz bandwidth of our 30 MHz transducer, we tested 20 and 40 MHz ultrasound (Supplementary Fig. 2a). Both showed similar suppression effects on neurons albeit the effect of the 40 MHz wave was weaker due to the greater attenuation coefficient in water and the 12.7 mm-long water path. We further tested the effect of amplitude modulation on the 30 MHz ultrasound. Experimentally, we applied pulsed modulation to the 30 MHz carrier signal and varied the duty cycle of the modulation. The data suggest that the reduced duty cycle gradually diminished the effect of neural modulation (Supplementary Fig. 2b) and the CW signal offered the strongest suppression to calcium transients. For the 10% duty cycle, we also varied the modulation frequency from 100 Hz to 100 kHz, which

made a minor difference to the results (Supplementary Fig. 2c). Finally, we tested using sinusoidal amplitude modulation and varied the modulation frequency from 0.5 MHz to 2 MHz, which also made little difference (Supplementary Fig. 2d). Overall, none of these modulated waveforms worked better than the CW high-frequency ultrasound.

As a control experiment, we performed the same modulation measurements on mice that expressed *Thy1*-YFP in neurons whose fluorescence emission was independent of the neuronal activity. The presence of the 30 MHz ultrasound did not affect the YFP fluorescence signals (Fig. 4a). We also tested moving the ultrasound transducer 5 mm away from the imaging FOV. As expected, the effect of the calcium transient suppression disappeared (Fig. 4b). The employed ultrasound intensity (I_{spta}: 2.17–4.46 W/cm^2, CW) in this study was a bit higher than the common medical ultrasound imaging intensity. To test whether the applied ultrasound could cause any damage to the brain tissue [18], we applied the 30 MHz ultrasound to the brain of *Cx3cr1*-EGFP mice that expressed EGFP in the microglia. Tissue damage would cause the aggregation of the microglia processes. Although much stronger ultrasound (I_{spta} reached 11.8 W/cm^2, CW) was employed in this control study, no microglia aggregation was observed (Fig. 4c). Moreover, we monitored the brain tissue temperature variation during the ultrasound modulating using miniature thermocouple sensors (PerfectPrime, TL0201, 0.1 mm), which showed less than 1 ∘C variation and negligible difference between awake and anesthetized mice (Supplementary Fig. 3).

In addition to calcium imaging, we further employed Electro-encephalogram (EEG) recording to monitor the neuronal population's response to the high-frequency ultrasound (Fig. 5a). Using wavelet transform, we decomposed the EEG signals into different frequency ranges (Fig. 5b). We found that the low frequency (0.3–1.3 Hz) activity was enhanced by the ultrasound wave while the high-frequency components largely remained the same (Fig. 5c). As a control measurement, we moved the ultrasound transducer 5 mm away from the EEG recording site. As expected, the EEG signal variation vanished (Fig. 5d). Next, we studied the EEG signal variation as a function of the applied ultrasound intensity. The data suggest that noticeable signal variation appeared when the ultrasound intensity rose above ~2 W/cm^2 (Fig. 5e), which agreed well with the two-photon calcium imaging results (Fig. 2a). Interestingly, the EEG signal variation would again disappear if the mice were under anesthesia (Fig. 5f), very similar to the observation by the calcium imaging (Fig. 1g). As the increased Delta wave and the suppression of neuronal activity can be correlated [47,48], the observed increase of the low-frequency EEG signal is consistent with the observation by the calcium imaging.

3. Discussion

The data from both the calcium imaging and the EEG recording suggest that the high frequency (~30 MHz) ultrasound can modulate neuronal activities, effectively shrinking the neural modulation volume by orders of magnitude. This will provide significantly improved resolutions and degrees of freedom for neural modulation. The spatial confinement of the ultrasound modulation in this work was limited by the numerical aperture (NA 0.24) of the off-the-shelf transducer. Further improvement on the focusing lenses (e.g. customizing

NA 0.5 ultrasound lenses) may potentially achieve even better resolutions, which would be highly valuable for modulating individual function regions in the small rodents' brains.

Limited by the transducer bandwidth, the highest ultrasound frequency applied was 40 MHz [49]. To achieve even greater spatial resolution, higher frequencies (e.g. 60 MHz) should be tested in future studies, which could further reduce the modulation volume at the expense of a reduced penetration depth. On the lower frequency side, the 20 MHz explored in this study offers much improved penetration (e.g. above centimeter) [50,51], which is sufficient to access the majority of the brain of common rodent models.

Compared to the common 1 MHz ultrasound [52,53], a key limitation of the 30 MHz ultrasound is that it will suffer from stronger loss through thick skulls (e.g. human skull) [54–56]. Therefore, it may not be able to achieve noninvasive transcranial performance on the human brain [57–59]. However, the attenuation through the mouse skull (Supplementary Table 1) is moderate and can be compensated by increasing the transducer input power. Therefore, high-frequency neural modulation can be implemented on mouse brain noninvasively. For bigger mammal models with thick skulls, the alternative solution is to perform surgery to replace part of the skull with plastic that matches the brain tissue in acoustic impedance, similar to the plastic cranial window with ~90% power transmission employed in this work.

A constraint in the employed dual-modality system is that the ultrasound focus was only applied to one location. Changing the ultrasound focus required manually adjusting a 3-axis linear stage. Potentially, customized high-frequency ultrasound transducer arrays should be employed to achieve arbitrary simultaneous multifoci 3D neural modulation.

In summary, we present the experimental results acquired by a dual-modality system combining two-photon calcium imaging and high-frequency focused ultrasound. The calcium imaging data suggest that the 30 MHz ultrasound can effectively suppress the calcium transients in awake mice. However, such an effect would disappear when the mice were under anesthesia. Additionally, the EEG measurement showed that the ultrasound increased the low-frequency EEG signals. The effect would disappear when the mice were under anesthesia, similar to the observation by the two-photon calcium imaging. Moreover, the minimum ultrasound intensity (~2 W/cm^2) required to cause EEG signal variation also agreed well with that of the calcium measurement. As a variety of neurological disorders such as epilepsy [60,61], Alzheimer's disease [62–64], and neuropathic pain [65–68] are associated with hyperactive neuronal activities, the capabilities of noninvasively suppressing neuronal responses are highly desirable for treatment and symptom alleviation. The *in vivo* results revealed in this study indicate that the ~30 MHz ultrasound can be employed for reliable neural suppression, paving the way for high-resolution neural activity control in neuroscience research and potential medical applications. Moreover, the dual-modality system developed and validated in this study will serve as a general platform for studying neuronal, glial, and vasculature dynamics induced by various ultrasound modulations.

4. Methods

4.1. Animal preparation

The wild type C57BL/6 mice, the *Thy1*-YFP mice, and the *Cx3cr1*-EGFP mice were all purchased from the Jackson Laboratories. For calcium imaging, we injected AAV1-*Syn*-GCaMP6s-WPRE375-SV40 virus (Addgene, 100843-AAV1, 1×10^{13}) into the visual cortex of the C57BL/6 mice 2–3 weeks before the *in vivo* imaging experiments. The cranial window surgeries were performed a few days before the imaging. The exposed cortex was covered by a 3 mm diameter plastic coverslip that was attached to the skull. For the vascular labeling, Dextran & Texas Red (70,000 MW, 5%, 50 mg/kg, Thermo Fisher) was employed through orbital injection. All procedures involving mice were approved by the Animal Care and Use Committees of Purdue University.

4.2. Installation of the water container

Different from the common calcium imaging implementation, we need to support a long water path for the 30 MHz transducer which featured a 12.7 mm-long working distance. This involves custom machined base support, large diameter head bar (1.8 g in weight), O-ring (0.5 mm and 32 mm in height and diameter, respectively), and water container (Supplementary Fig. 4). First, we put the extrusions of the head bar into the indentation on the base support. Next, we placed the O-ring on the outer edge of the head bar, then pressed the O-ring onto the head bar with the water container above, and finally locked the container position using two low-profile 8–32 machine screws. The pressed O-ring ensured a watertight connection from the head bar to the water container. The base support was attached to a 3-axis motorized stage (LTA-HL, Newport) which precisely positioned the mouse under the imaging system.

4.3. In vivo two-photon imaging and data analysis

The calcium imaging data were primarily collected from layer 2/3 neurons of the visual cortex. We also tested the motor cortex which showed the same effects (Supplementary Fig. 5). The calcium image recording rate was 4 Hz. The typical recording session was 300 s long. In the first 60 s, the ultrasound was off (recording baseline activity). In the next 60 s, the ultrasound was on (modulation). In the last 180 s, the ultrasound was off (recovery). Before extracting the calcium transients from the somata, we utilized the average of the time-lapsed images as the position reference and performed spatial cross-correlations for motion correction. We employed normalized heatmaps to assist the visualization of neuronal activity (e.g. Figs. 1e, 2a and 3c, Supplementary Fig. 2), in which the calcium activity ($\Delta F/F_0$) of each neuron was normalized by its maximum value and the neurons were ordered according to the time of maximum $\Delta F/F_0$ responses. The minimum 10% of each cell's fluorescence signal was defined as F_0. The threshold for detecting calcium transient was for $\Delta F/F_0 > 0.5$. The full width at half maximum (FWHM) of each calcium transient was measured as the calcium transient duration [69]. The frequency was defined as the number of calcium transients per second and the peak value was defined as the maximum value within each calcium transient. The total calcium activity was defined as the accumulated area under the curve per second.

4.4. Electroencephalogram (EEG) recording and data analysis

EEG signals were recorded by using an integrated data acquisition and analysis system (BL-420F, TME technology). The electrode was made from an epoxy coated silver wire (0.076 mm in diameter). The electrodes were carefully inserted into the V1 cortex which was then covered by a plastic coverslip. Before the EEG recording, we translated the brain under the two-photon microscope such that the electrodes were at the center of the focal plane to ensure that the electrodes were near the ultrasound modulation zone. The wavelet-based signal decomposition was implemented by using the wavelet toolbox of MATLAB (MathWorks).

4.5. Statistics

All the data in this study are represented as mean ± standard error. All the data analysis was performed with the Shapiro-Wilk normality test. For the data that passed the normality test ($P > 0.05$), an unpaired t-test with Welch's correction was selected for two groups' comparison, the one or two-way ANOVA Tukey's or Sidak's multiple comparisons test were selected for comparing multiple groups. $P < 0.05$ is recognized as statistically significant. All statistical analyses were performed using *GraphPad Prism*. No results of the successful acquisition from images and measurements were excluded and filtered. The experiment did not include randomized and blinding experiments. At least three mice were used in each experiment. P values, n, and the statistical tests for all the experiments were summarized in Supplementary Table 2.

Supplementary Material

Refer to Web version on PubMed Central for supplementary material.

Acknowledgment

This work was funded by NIH (U01NS118302, U01NS107689) and Purdue University. M.C. thanks Howard Hughes Medical Institute for scientific instruments. Q.Z. acknowledges the support by NIH R01EY030126. Z.C. thanks Baoling Lai (NYU Langone Health Center) for valuable comments and discussion.

Data availability

The datasets generated during and/or analyzed during the current study are available from the corresponding author on reasonable request.

References

[1]. Schwalb JM, Hamani C. The history and future of deep brain stimulation. Neurotherapeutics 2008;5:3–13. [PubMed: 18164479]

[2]. Ressler KJ, Mayberg HS. Targeting abnormal neural circuits in mood and anxiety disorders: from the laboratory to the clinic. Nat Neurosci 2007;10: 1116–24. [PubMed: 17726478]

[3]. Deisseroth K. Optogenetics. Nat Methods 2011;8:26–9. [PubMed: 21191368]

[4]. Kubanek J, Shukla P, Das A, Baccus SA, Goodman MB. Ultrasound elicits behavioral responses through mechanical effects on neurons and ion channels in a simple nervous system. J Neurosci 2018;38:3081–91. [PubMed: 29463641]

[5]. Bystritsky A, et al. A review of low-intensity focused ultrasound pulsation. Brain Stimul 2011;4:125–36. [PubMed: 21777872]

[6]. Hallett M Transcranial magnetic stimulation: a primer. Neuron 2007;55: 187–99. [PubMed: 17640522]

[7]. Sato T, Shapiro MG, Tsao DY. Ultrasonic neuromodulation causes widespread cortical activation via an indirect auditory mechanism. Neuron 2018;98: 1031–41. e1035. [PubMed: 29804920]

[8]. Tyler WJ, Lani SW, Hwang GM. Ultrasonic modulation of neural circuit activity. Curr Opin Neurobiol 2018;50:222–31. [PubMed: 29674264]

[9]. Tufail Y, Yoshihiro A, Pati S, Li MM, Tyler WJ. Ultrasonic neuromodulation by brain stimulation with transcranial ultrasound. Nat Protoc 2011;6:1453–70. [PubMed: 21886108]

[10]. Fry F, Ades H, Fry W. Production of reversible changes in the central nervous system by ultrasound. Science 1958;127:83–4. [PubMed: 13495483]

[11]. Tufail Y, et al. Transcranial pulsed ultrasound stimulates intact brain circuits. Neuron 2010;66:681–94. [PubMed: 20547127]

[12]. Estrada H, Özbek A, Robin J, Shoham S, Razansky D. Spherical array system for high-precision transcranial ultrasound stimulation and optoacoustic imaging in rodents. IEEE Trans Ultrason Ferroelectrics Freq Control 2020;68:107–15.

[13]. Tran T, Roger S, Le Guennec J-Y, Tranquart F, Bouakaz A. Effect of ultrasound-activated microbubbles on the cell electrophysiological properties. Ultrasound Med Biol 2007;33:158–63. [PubMed: 17189059]

[14]. Guo H, et al. Ultrasound produces extensive brain activation via a cochlear pathway. Neuron 2018;98:1020–30. e1024. [PubMed: 29804919]

[15]. Krasovitski B, Frenkel V, Shoham S, Kimmel E. Intramembrane cavitation as a unifying mechanism for ultrasound-induced bioeffects. Proc Natl Acad Sci Unit States Am 2011;108:3258–63.

[16]. Plaksin M, Shoham S, Kimmel E. Intramembrane cavitation as a predictive biopiezoelectric mechanism for ultrasonic brain stimulation. Phys Rev X 2014;4: 011004.

[17]. Ibsen S, Tong A, Schutt C, Esener S, Chalasani SH. Sonogenetics is a non-invasive approach to activating neurons in Caenorhabditis elegans. Nat Commun 2015;6:1–12.

[18]. Blackmore J, Shrivastava S, Sallet J, Butler CR, Cleveland RO. Ultrasound neuromodulation: a review of results, mechanisms and safety. Ultrasound Med Biol 2019;45:1509–36. [PubMed: 31109842]

[19]. Tyler WJ, et al. Remote excitation of neuronal circuits using low-intensity, low-frequency ultrasound. PLoS One 2008;3:e3511. [PubMed: 18958151]

[20]. Tyler WJ. In 2017 IEEE international ultrasonics symposium, IUS 2017 8092717. IEEE Computer Society; 2017.

[21]. Kamimura HA, et al. Focused ultrasound neuromodulation of cortical and subcortical brain structures using 1.9 MHz. Med Phys 2016;43:5730–5. [PubMed: 27782686]

[22]. Plaksin M, Kimmel E, Shoham S. Cell-type-selective effects of intramembrane cavitation as a unifying theoretical framework for ultrasonic neuromodulation. Eneuro 2016;3.

[23]. Foster FS, Pavlin CJ, Harasiewicz KA, Christopher DA, Turnbull DH. Advances in ultrasound biomicroscopy. Ultrasound Med Biol 2000;26:1–27. [PubMed: 10687788]

[24]. Mohammadjavadi M, et al. Elimination of peripheral auditory pathway activation does not affect motor responses from ultrasound neuromodulation. Brain Stimul 2019;12:901–10. [PubMed: 30880027]

[25]. Estrada H, Rebling J, Turner J, Razansky D. Broadband acoustic properties of a murine skull. Phys Med Biol 2016;61:1932. [PubMed: 26878583]

[26]. Yoo S-S, et al. Focused ultrasound modulates region-specific brain activity. Neuroimage 2011;56:1267–75. [PubMed: 21354315]

[27]. Menz MD, Oralkan Ö, Khuri-Yakub PT, Baccus SA. Precise neural stimulation in the retina using focused ultrasound. J Neurosci 2013;33:4550–60. [PubMed: 23467371]

[28]. Yao T, Yu S, Liu Y, Yuan B. In vivo ultrasound-switchable fluorescence imaging. Sci Rep 2019;9:1–13. [PubMed: 30626917]

[29]. Kubanek J Neuromodulation with transcranial focused ultrasound. Neurosurg Focus 2018;44:E14.

[30]. Aurup C, Kamimura HA, Konofagou EE. High-resolution focused ultrasound neuromodulation induces limb-specific motor responses in mice in vivo. Ultrasound Med Biol 2021;47:998–1013. [PubMed: 33455808]

[31]. Yu K, Niu X, Krook-Magnuson E, He B. Intrinsic functional neuron-type selectivity of transcranial focused ultrasound neuromodulation. Nat Commun 2021;12:1–17. [PubMed: 33397941]

[32]. Kim S, et al. Transcranial focused ultrasound stimulation with high spatial resolution. Brain Stimul 2021;14:290–300. [PubMed: 33450428]

[33]. Mehić E, et al. Increased anatomical specificity of neuromodulation via modulated focused ultrasound. PLoS One 2014;9:e86939. [PubMed: 24504255]

[34]. Foley JL, Little JW, Vaezy S. Effects of high-intensity focused ultrasound on nerve conduction. Muscle Nerve: Off J Am Assoc Electrodiagnos Med 2008;37: 241–50.

[35]. Legon W, et al. Transcranial focused ultrasound modulates the activity of primary somatosensory cortex in humans. Nat Neurosci 2014;17:322–9. [PubMed: 24413698]

[36]. Scarcelli T, et al. Stimulation of hippocampal neurogenesis by transcranial focused ultrasound and microbubbles in adult mice. Brain Stimul 2014;7: 304–7. [PubMed: 24629831]

[37]. Li G-F, et al. Improved anatomical specificity of non-invasive neuro-stimulation by high frequency (5 MHz) ultrasound. Sci Rep 2016;6:1–11. [PubMed: 28442746]

[38]. Cannata JM, Williams JA, Zhou Q, Ritter TA, Shung KK. Development of a 35-MHz piezo-composite ultrasound array for medical imaging. IEEE Trans Ultrason Ferroelectrics Freq Control 2006;53:224–36.

[39]. Menz MD, et al. Radiation force as a physical mechanism for ultrasonic neurostimulation of the ex vivo retina. J Neurosci 2019;39:6251–64. [PubMed: 31196935]

[40]. Ye J, et al. Ultrasonic control of neural activity through activation of the mechanosensitive channel MscL. Nano Lett 2018;18:4148–55. [PubMed: 29916253]

[41]. Verhagen L, et al. Offline impact of transcranial focused ultrasound on cortical activation in primates. Elife 2019;8:e40541. [PubMed: 30747105]

[42]. Folloni D, et al. Manipulation of subcortical and deep cortical activity in the primate brain using transcranial focused ultrasound stimulation. Neuron 2019;101:1109–16. e1105. [PubMed: 30765166]

[43]. Manuel TJ, et al. Ultrasound neuromodulation depends on pulse repetition frequency and can modulate inhibitory effects of TTX. Sci Rep 2020;10:1–10. [PubMed: 31913322]

[44]. Thrane AS, et al. General anesthesia selectively disrupts astrocyte calcium signaling in the awake mouse cortex. Proc Natl Acad Sci Unit States Am 2012;109:18974–9.

[45]. Hemmings HC, Yan W, Westphalen RI, Ryan TA. The general anesthetic isoflurane depresses synaptic vesicle exocytosis. Mol Pharmacol 2005;67: 1591–9. [PubMed: 15728262]

[46]. Chen C, et al. Long-term imaging of dorsal root ganglia in awake behaving mice. Nat Commun 2019;10:1–11. [PubMed: 30602773]

[47]. Brown RE, Basheer R, McKenna JT, Strecker RE, McCarley RW. Control of sleep and wakefulness. Physiological reviews; 2012.

[48]. Herrera CG, et al. Hypothalamic feedforward inhibition of thalamocortical network controls arousal and consciousness. Nat Neurosci 2016;19:290–8. [PubMed: 26691833]

[49]. Prieto ML, Firouzi K, Khuri-Yakub BT, Madison DV, Maduke M. Spike frequency–dependent inhibition and excitation of neural activity by high-frequency ultrasound. J Gen Physiol 2020;152:e202012672. [PubMed: 33074301]

[50]. Shung KK. High frequency ultrasonic imaging. J Med Ultrasound 2009;17: 25–30. [PubMed: 20445825]

[51]. Goss S, Frizzell L, Dunn F. Ultrasonic absorption and attenuation in mammalian tissues. Ultrasound Med Biol 1979;5:181–6. [PubMed: 556199]

[52]. Legon W, Bansal P, Tyshynsky R, Ai L, Mueller JK. Transcranial focused ultrasound neuromodulation of the human primary motor cortex. Sci Rep 2018;8:1–14. [PubMed: 29311619]

[53]. Ye PP, Brown JR, Pauly KB. Frequency dependence of ultrasound neurostimulation in the mouse brain. Ultrasound Med Biol 2016;42:1512–30. [PubMed: 27090861]

[54]. Estrada H, et al. In photons plus ultrasound: imaging and sensing 2016, 9708 97080M International Society for Optics and Photonics; 2016.

[55]. Konofagou EE. Optimization of the ultrasound-induced blood-brain barrier opening. Theranostics 2012;2:1223. [PubMed: 23382778]

[56]. Legon W, Ai L, Bansal P, Mueller JK. Neuromodulation with single-element transcranial focused ultrasound in human thalamus. Hum Brain Mapp 2018;39:1995–2006. [PubMed: 29380485]

[57]. Gt Haar. Ultrasonic imaging: safety considerations. Interface focus 2011;1: 686–97. [PubMed: 22866238]

[58]. Nelson TR, Fowlkes JB, Abramowicz JS, Church CC. Ultrasound biosafety considerations for the practicing sonographer and sonologist 2009.

[59]. Fomenko A, Neudorfer C, Dallapiazza RF, Kalia SK, Lozano AM. Low-intensity ultrasound neuromodulation: an overview of mechanisms and emerging human applications. Brain Stimul 2018;11:1209–17. [PubMed: 30166265]

[60]. Devinsky O, et al. Epilepsy. Nat Rev Dis Prim 2018;4:18024. [PubMed: 29722352]

[61]. Scharfman HE. The neurobiology of epilepsy. Curr Neurol Neurosci Rep 2007;7:348–54. [PubMed: 17618543]

[62]. Nuriel T, et al. Neuronal hyperactivity due to loss of inhibitory tone in APOE4 mice lacking Alzheimer's disease-like pathology. Nat Commun 2017;8:1–14. [PubMed: 28232747]

[63]. Ghatak S, et al. Mechanisms of hyperexcitability in Alzheimer's disease hiPSC-derived neurons and cerebral organoids vs isogenic controls. Elife 2019;8: e50333. [PubMed: 31782729]

[64]. Šišková Z, et al. Dendritic structural degeneration is functionally linked to cellular hyperexcitability in a mouse model of Alzheimer's disease. Neuron 2014;84:1023–33. [PubMed: 25456500]

[65]. Baron R Mechanisms of disease: neuropathic pain—a clinical perspective. Nat Clin Pract Neurol 2006;2:95–106. [PubMed: 16932531]

[66]. Gwak YS, Hulsebosch CE. Neuronal hyperexcitability: a substrate for central neuropathic pain after spinal cord injury. Curr Pain Headache Rep 2011;15: 215–22. [PubMed: 21387163]

[67]. Colloca L, et al. Neuropathic pain. Nat Rev Dis Prim 2017;3:1–19.

[68]. Darrow DP. Focused ultrasound for neuromodulation. Neurotherapeutics 2019;16:88–99. [PubMed: 30488340]

[69]. Li W, Ma L, Yang G, Gan W-B. REM sleep selectively prunes and maintains new synapses in development and learning. Nat Neurosci 2017;20:427–37. [PubMed: 28092659]

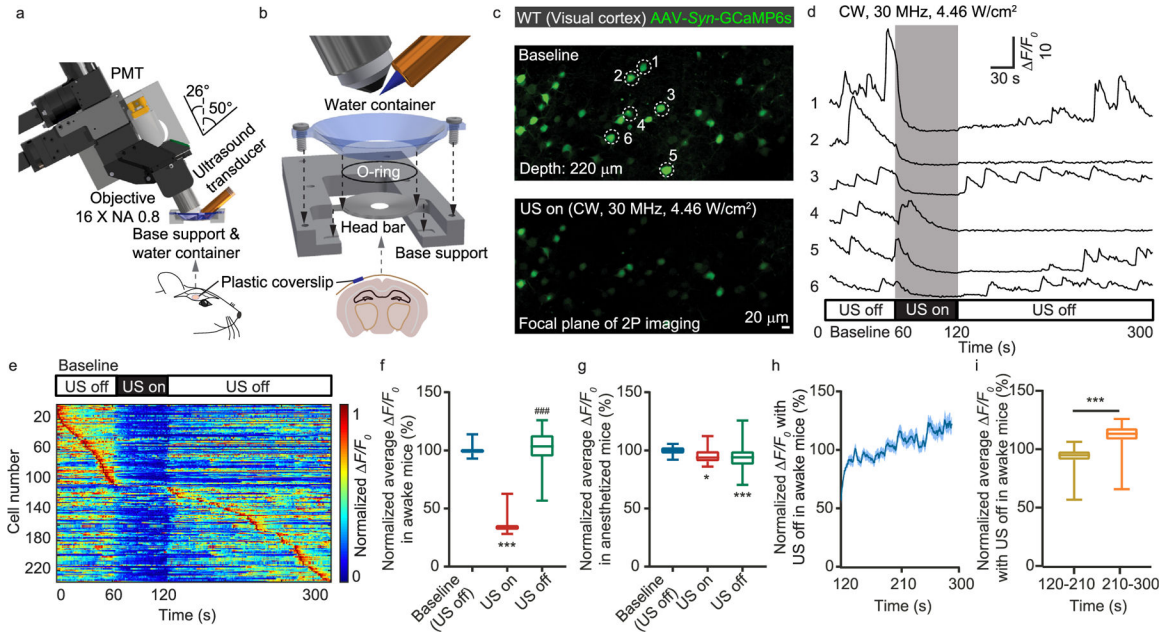

Fig. 1.

System and implementation of simultaneous ultrasound modulation and two-photon calcium imaging. (a) System design of the dual-modality system combining a two-photon laser scanning fluorescence microscope and a 30 MHz polymer ultrasound transducer. (b) The mechanical assembly including the head bar, O-ring, water container, and base support. (c) Representative two-photon calcium imaging of mouse visual cortex without and with ultrasound modulation. (d) Calcium transient traces for the neurons labeled in c. (e) Maximum-normalized calcium activity. (f) Statistics of $\Delta F/F_0$ before, during, and after ultrasound modulation for awake mice. (g) Statistics of $\Delta F/F_0$ before, during, and after ultrasound modulation for mice in anesthesia. (h) The recovering of the calcium activity in awake mice over time after the ultrasound was turned off. (i) Statistics of $\Delta F/F_0$ during the initial and the subsequent 90 s after the ultrasound was turned off in awake mice. $^{**}P < 0.01$, *** or $^{\#\#\#}P < 0.001$.

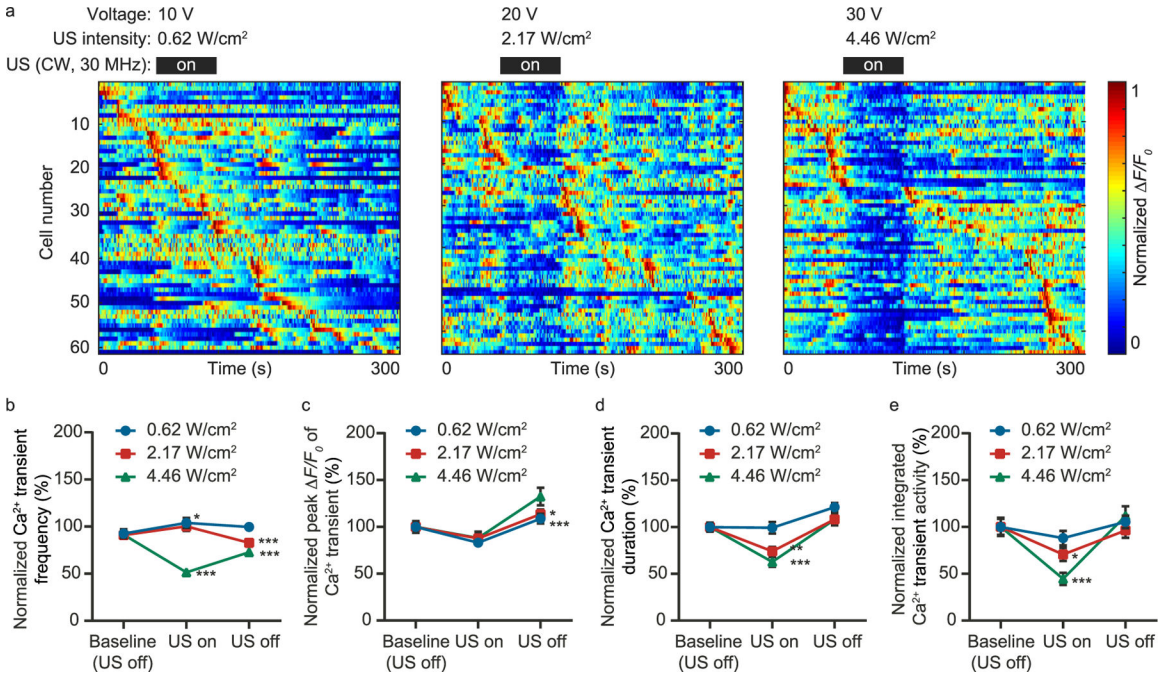

Fig. 2.

Quantify the ultrasound intensity required for the calcium transient suppression. (a) Maximum-normalized calcium activity measured with different ultrasound intensity. The corresponding applied voltage and ultrasound intensity are shown for each measurement. (b–e) Statistics of the calcium transient frequency, peak $\Delta F/F_0$, duration, and integrated activity, respectively. $*P < 0.05$, $**P < 0.01$, $***P < 0.001$.

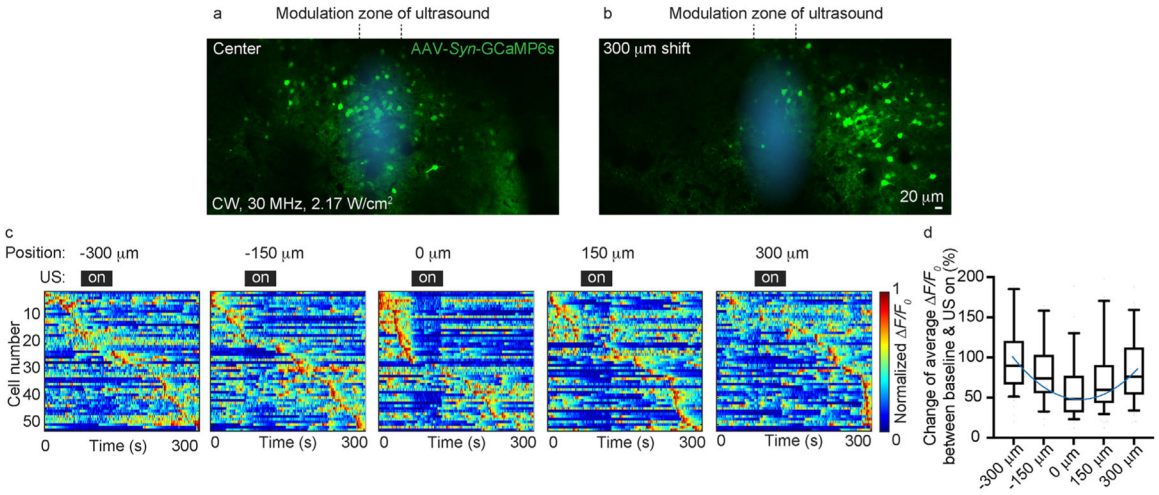

Fig. 3.

Quantify the spatial resolution of the high-frequency ultrasound neural modulation. (a, b) Representative calcium images before and after the horizontal translation of the brain. (c) Maximum-normalized calcium activity of the same neuronal population measured with different horizontal translation. (d) Quantification of calcium activity as a function of horizontal translation distances.

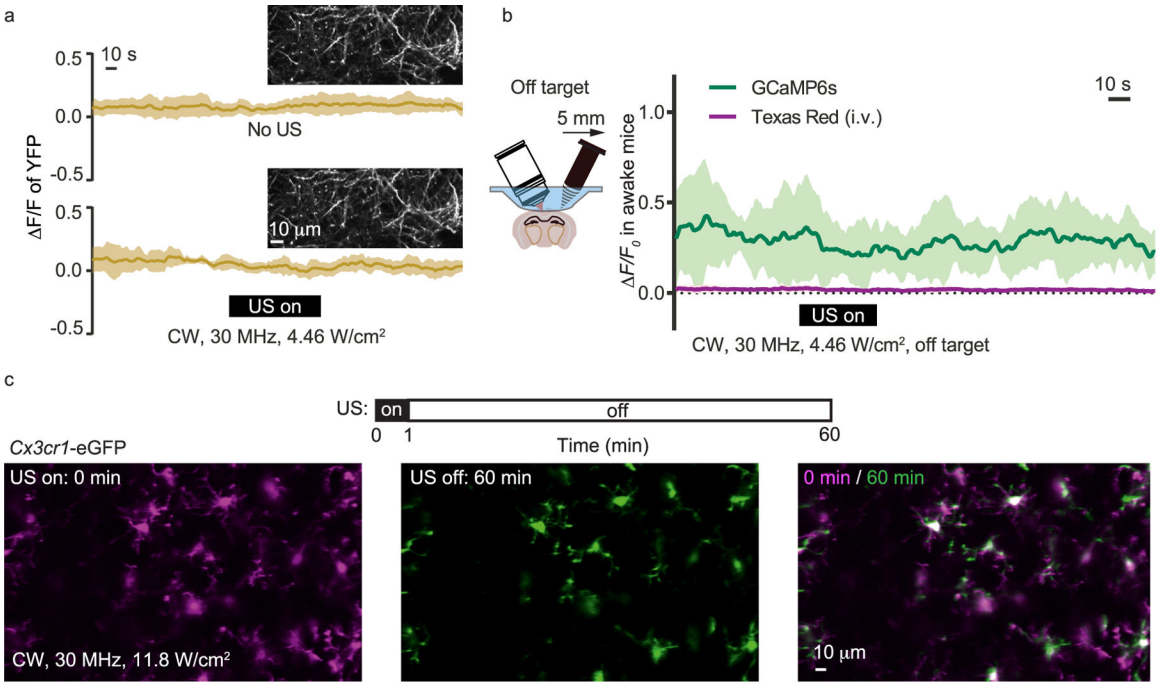

Fig. 4.

Control studies with YFP, GCaMP6s and Cx3cr1 mice. (a) Fluorescence signal of the *Thy1*-YFP expressing neurons without and with the 30 MHz ultrasound modulation. (b) Calcium imaging with the ultrasound transducer moved 5 mm away from the imaging region. The blood vessels were also visualized by the Texas Red labeling. (c) *Cx3cr1*-EGFP mice imaging with ultrasound modulation. The applied ultrasound intensity (11.8 W/cm^2) was significantly greater than the typical value used in this study. (For interpretation of the references to colour in this figure legend, the reader is referred to the Web version of this article.)

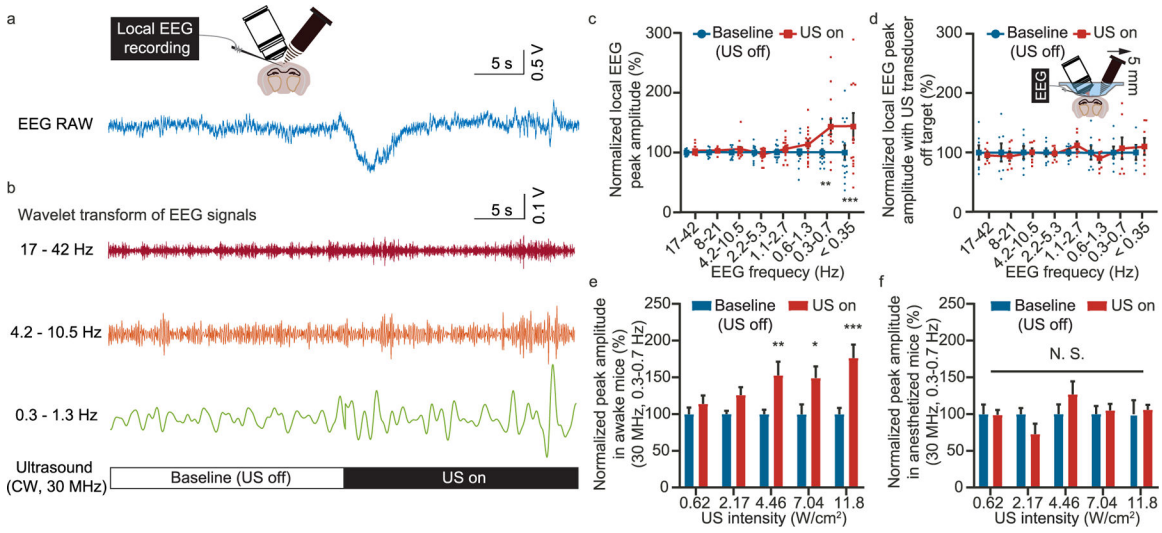

Fig. 5.

Simultaneous EEG recording during high-frequency ultrasound modulation. (a) Representative raw data of the EEG recording. (b) EEG signals decomposed to different frequency range by wavelet transform. (c) Statistics of the EEG peak amplitude as a function of frequency range before and after the ultrasound modulation. (d) Statistics of the EEG peak amplitude as a function of frequency before and after the ultrasound modulation with the ultrasound transducer moved 5 mm away. (e) Statistics of the peak amplitude for 0.3–0.7 Hz EEG signal with ultrasound of different intensity applied to awake mice. (f) Statistics of the peak amplitude for 0.3e0.7 Hz EEG signal with ultrasound of different intensity applied to anesthetized mice. $*P < 0.05$, $**P < 0.01$, $***P < 0.001$.